Distribution Categories:
Coal Conversion and Utilization--
Coal Science and Analysis (UC-90a)

ANL/FE-85-07

ANL-FE--85-07

DE87 000281

ARGONNE NATIONAL LABORATORY
9700 South Cass Avenue
Argonne, Illinois 60439

DEVELOPMENT OF ACOUSTIC FLOW INSTRUMENTS FOR SOLID/GAS PIPE FLOWS

by

S. H. Sheen and A. C. Raptis

Components Technology Division

May 1986

Prepared for U. S. Department of Energy
Office of Fossil Energy, Morgantown Energy Technology Center
Under Advanced Research
in Instrumentation and Control Technology
FTP 49644

Argonne National Laboratory, with facilities in the states of Illinois and Idaho, is owned by the United States government, and operated by The University of Chicago under the provisions of a contract with the Department of Energy.

Printed in the United States of America
Available from
National Technical Information Service
U. S. Department of Commerce
5285 Port Royal Road
Springfield, VA 22161

NTIS price codes
Printed copy: A03
Microfiche copy: A01

CONTENTS

FIGURES

TABLES

DEVELOPMENT OF ACOUSTIC FLOW INSTRUMENTS FOR SOLID/GAS PIPE FLOWS

by

S. H. Sheen and A. C. Raptis

ABSTRACT

Two nonintrusive acoustic flow sensing techniques are reported. One technique, passive in nature, simply measures the bandpassed acoustic noise level produced by particle/particle and particle/wall collisions. The noise levels, given in true RMS voltages or in autocorrelations, show a linear relationship to particle velocity but increase with solid concentration. Therefore, the passive technique requires calibration and a separate measure of solid concentration before it can be used to monitor the particle velocity. The second technique is based on the active cross-correlation principle. It measures particle velocity directly by correlating flow-related signatures at two sensing stations. The velocity data obtained by this technique are compared with measurements by a radioactive-particle time-of-flight (TOF) method. A multiplier of 1.53 is required to bring the acoustic data into agreement with the radioactive TOF result. The difference may originate from the difference in flow fields where particles are detected. The radioactive method senses particles mainly in the turbulent region and essentially measures average particle velocity across the pipe, while the acoustic technique detects particles near the pipe wall, and so measures the particle velocity in the viscous sublayer. Both techniques were tested in flows of limestone and air and 1-mm glass beads and air at the Argonne National Laboratory Solid/Gas Test Facility (SGFTF). The test matrix covered solid velocities of 20 to 30 m/s in a 2-in. pipe and solid-to-gas loading ratios of 6 to 22.

1. INTRODUCTION

This document reports progress since 1982 on the development of acoustic techniques for measuring solid/gas flowrates. The purpose of the program is to develop nonintrusive advanced sensing techniques that can measure solids feedrate in a hostile coal gasification environment. Typically, coal particles are transported pneumatically in coal mining and coal conversion processes. Measurement of coal particle velocity and loading in such a transporting line is very important to safe, efficient operation of a coal plant. But on-line continuous particle velocity monitoring is still a difficult task. Available techniques remain at the

research stage with limited industrial application.

Commonly employed techniques comprise the radioactive tracer method [1], optical techniques [2], electromagnetic methods [3,4], and conventional mechanical approaches [5,6]. Use of radioactive tracers provides a direct measurement of particle velocity, but the technique requires a nuclear power source, which limits the technique to research applications. Laser doppler anemometry (LDA) has made the optical technique a promising diagnostic method for two-phase flows. However, the requirement of an optical window has hampered its industrial use, especially in coal processes. Conventional mechanical methods are typically intrusive in nature. For example, an isokinetic sampling technique for particle velocity measurement applies only for a very dilute solid suspension with small particle size because of intrusion and plugging problems. Electromagnetic methods are based on either electrostatic induction of charges on particles or changes of electrical capacitance as particles pass through an electrical field. Nieh et al. [7] recently reported measurements of particle velocity and velocity profile by an electrostatic induction probe. Again, application of such a probe is limited to a very dilute solid suspension. The most promising technique in industrial applications is the capacitance method, which measures the particle transit time by cross-correlating the capacitance variation detected at two sensing electrodes separated by a known distance and senses the solid loading from the capacitance change resulting from the change of dielectric constant of the medium. The capacitance technique, however, needs a test section made of insulating material such as ceramics.

Most of the available techniques (except the capacitance method) are either impractical or unacceptable to the coal industry, which normally transports coal at high solid-to-gas loading ratios and recycles ash particles under high temperature and pressure. The ideal technique must be able to survive this hostile environment, and be nonintrusive and responsive to a wide range of solid-to-gas loading ratios.

Argonne National Laboratory (ANL), under contract to the U. S. Department of Energy, has been developing advanced techniques to measure mass flowrate of solid/gas flows. Two techniques, capacitive [4] and acoustic, have been the focus of the program. Acoustic/ultrasonic methods have been widely used in industrial process controls. For example, flow velocity measurements for solid/liquid flows have been successfully developed under the Doppler [8] and active cross-correlation [9] principles. However, for solid/gas flows, the same principles are difficult to implement because of (1) high acoustic attenuation in gases, (2) high particle impingement noise, and (3) problems associated with acoustic impedance mismatch.

In this report we describe two potential acoustic techniques that rely on the acoustic noise produced by the particle/particle and particle/wall interactions.

One technique measures noise level directly.

The other-- a new technique developed at ANL-- applies the cross-correlation approach.

Both techniques were evaluated in a series of flow tests at the ANL Solid/Gas Flow Test Facility (SGFTF) [10]. Results are compiled in this report and qualitatively interpreted by simple theoretical models to justify the relation between acoustic noise and flowrate.

2. ANL SOLID/GAS FLOW TEST FACILITY

The SGFTF is described in detail in another ANL report [11]. The facility, shown in Fig. 1, is a closed system operating at near-ambient temperature and pressure. It consists of two storage hoppers mounted on electric scales, a dense-phase gravity feed leg, and a long dilute-phase test region. For the tests, capacitive and acoustic flow instruments were installed in the dilute-phase test region. During the first series of tests, without radioactive particle injection, the test region was only 2.4 m (8 ft) long and used 3 in. schedule 40 pipe. Later we found that the test region was too short for establishing a steady particle velocity. So during the radioactive particle injection tests, the test region was extended to 12 m (40 ft), and 2 in. pipe was used. The radioactive particle injection system is described in Ref. 12. Locations of gamma detectors and flow instruments are shown in Fig. 2; the acoustic instrument was about 7.6 m from the mixing tee.

During a normal test run, the solids feedrate was controlled by the opening of a 3 in. knife valve and the flowrate of the air, which could be supplied at up to 0.118 m^3/s (250 cubic feet per minute). The actual solids feedrate was measured from the hopper weight change recorded on the data acquisition system of the facility. With the mixing tee arrangement [13] used in the tests, we could control the mass flow between 0.09 and 1.8 kg/s (0.2 and 4.0 lb/s). Limestone and glass beads were used in the flow tests, both with an average particle diameter of 1 mm. For the limestone, the solid-to-air loading ratio was varied from 4 to 12; for the glass beads, the ratio was from 6 to 22.

3. ACOUSTIC FLOW SENSING TECHNIQUES

Acoustic and ultrasonic techniques have been widely applied to industrial process control and diagnosis, ranging from flow, temperature, and level measurements to nondestructive testing and inspection. The distinct advantage of these techniques is the nonintrusive sensing

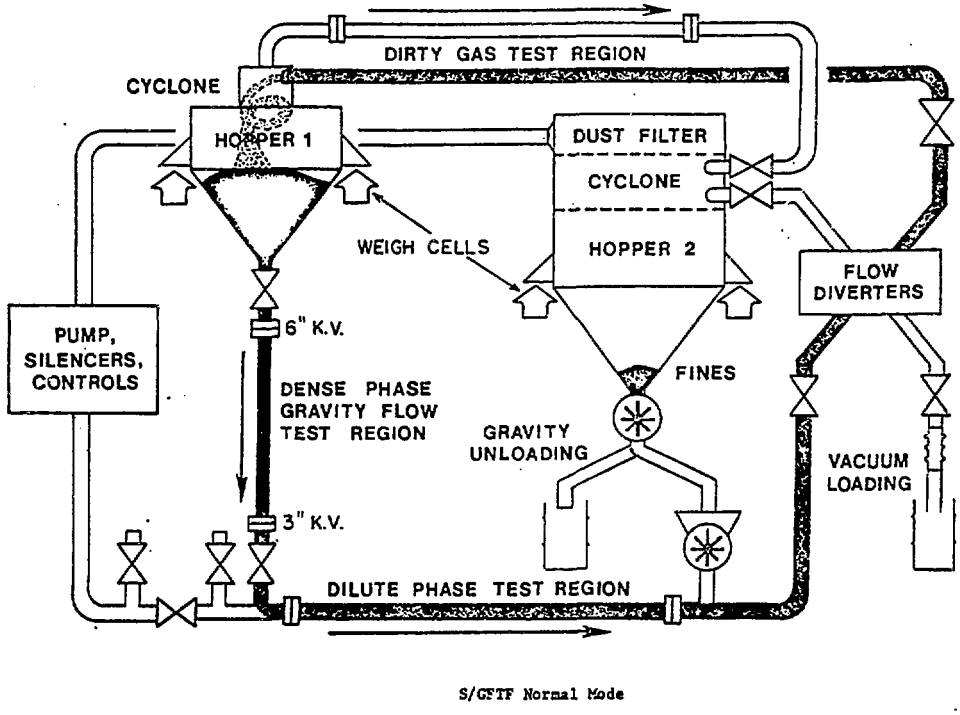

Fig. 1. Schematic of the SGFTF

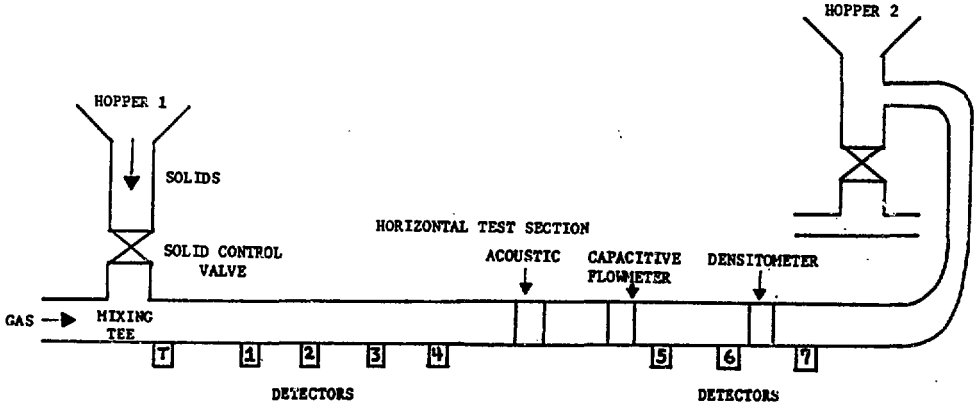

Device	Location From Mixing Tee (m)	Device	Location from Mixing Tee (m)
Trigger Detector	0.54	Densitometer 2	6.35
Detector 1	2.19	Acoustic Spoolpiece	7.61
Densitometer 1	2.71	Capacitive Flowmeter	8.93
Detector 2	3.21	Detector 5	9.58
Detector 3	4.46	Detector 6	10.92
Detector 4	5.71	Improved Densitometer, D3	11.57
		Detector 7	12.27

Fig. 2. Flow Instruments in the Test Section of the SGFTF

capability. Ultrasonic flow instruments for solid/liquid flows are the typical example; both Doppler and cross-correlation flowmeters developed [14] so far are of the nonintrusive and direct clamp-on type. However, application of such techniques to gaseous media is rather limited because of (1) high acoustic attenuation in gases (for example, at 100 kHz, about 3 dB/m in air compared with 10^{-4} dB/m in water) and (2) a large acoustic impedance difference between a gaseous medium and the pipe wall if the clamp-on arrangement is selected. The impedance mismatch restricts the amount of acoustic energy that can be transmitted in and out of the gas stream. This is why remote sensing, external to the pipe wall, on a gas stream is not recommended.

In addition to the two factors mentioned above, the noise level in a solid/gas flow must be considered. In comparison with solid/liquid flows, a significant increase in noise level is expected in a solid/gas stream because of higher flow velocity and noise produced directly by the particle/particle and particle/wall interactions, which depend on material properties of solids and pipe wall as well as piping arrangement. Therefore, any acoustic instrument that is to work in this noisy environment either requires a strong sound source or must make use of the noise itself.

3.1 SOLID/GAS PIPE FLOW NOISE

The feasibility of an acoustic technique normally is evaluated by use of the sonar equation approach to determine the optimum operating conditions. One of the variables in the sonar equation is the background noise level of the system being monitored. For solid/gas pipe flows, the background noise arises primarily from the impingement and scrubbing actions between solid particles and the pipe wall. In an earlier feasibility study [15], the solid/gas flow noise was estimated from gas pipeline noise [16] and power plant work area noise [17]. The estimate was about 70 dB re 1 μPa-Hz at 1 kHz, which decreases at 6 dB/octave, but this estimated noise level has not been verified experimentally.

Solid/gas flow noise can be considered a type of acoustic emission that occurs in a solid/gas suspension flow. Use of such acoustic emission for process monitoring of powder flow was reported by Arrington [18]. He found that the total mean square (TMS) voltage of the noise level was linearly proportional to the mass flowrate for very dilute suspensions, up to 1.4×10^{-3} kg/s. The first demonstrated use of flow noise to diagnose a coal process stream was by Roach et al. [19] at the BIGAS pilot plant. They built a flow/no-flow indicator and tested it on a char return line at the BIGAS coal gasifier. (The instrument detects the char particle flow from the flow noise variation.) Roach et al. found that the steam noise in the char return line dominated the acoustic background and was attenuated in the presence of char particles. Subsequently, a char density meter was proposed based on the noise level change.

Measurement of noise level is a passive technique. It requires only a

wideband transducer (or microphone), which can be mounted on the outside of the pipe wall or in direct contact with the flow. Both sensing arrangements were tested at ANL. Figure 3 shows the acoustic test section, which consists of three ANL high-temperature microphones [20] exposed to the solid/gas flow through 7/8-in. openings and two clamp-on transducers isolated from the flow by acoustic windows. The microphone has a flat frequency response up to 100 kHz but its acoustic impedance is constructed to match liquids (~1.5 x 10^5 g/cm^2-s). The acoustic windows are made of either stainless steel (acoustic impedance Z_s = 4.45 x 10^6 g/cm^2-s) or teflon (Z_t = 0.3 x 10^6 g/cm^2-s). The mismatch in the acoustic impedance limits the amount of acoustic energy transfer between the gas flow and pipe wall.

Figure 4 shows the signal conditioning and analysis system. Charge amplifiers were used to condition the microphone signals, while voltage amplifiers were used for the transducers. High-pass filters followed the amplifiers to eliminate any low-frequency mechanical noise, such as pipe vibration, which can be predetermined from accelerometer measurement. Then signals were analyzed by a true root-mean-square (RMS) voltmeter or a wide-band spectrum analyzer (SD360). To assure absolute noise level measurement, before installation the ANL microphones were calibrated in water against a hydrophone. The average sensitivity of the three chosen microphones was 1900 pc/bar or -154 dB re 1pc/1μPa.

3.1.1 Limestone/Air Flow Tests

A series of limestone/air flow tests was conducted at the SGFTF, which had a 2.4 m long dilute-phase test region; 3 in. pipe was used in most test regions except near the ANL capacitive flow instrument [22], where a 2 in. pipe was used. The acoustic test section was installed upstream of the capacitive instrument near the mixing tee, where limestone particles were in the initial accelerating stage. The average limestone diameter was 1 mm, but because of attrition, the diameter decreased during circulation. To maintain roughly the same limestone size distribution, the powdered-form limestone was filtered out and replaced by new limestone after each test run.

The test conditions are given in Table 1. The solids feedrate and the air flowrate were measured from, respectively, the hopper 1 weight change and an orifice plate flowmeter located upstream of the mixing tee. Both measurements had an accuracy of 5%; about 10% variation in solids feedrate was normally expected during each run.

Figure 5 shows two spectra, up to 50 kHz (spectra between 40 kHz and 50 kHz were attenuated by the aliasing filter of the analyzer) of the microphone signals detected during the test of 0.45 kg/s and 0.076 m^3/s air flowrate. The spectra show the difference in noise between air flow and limestone/air flow. The presence of limestone particles increased the power

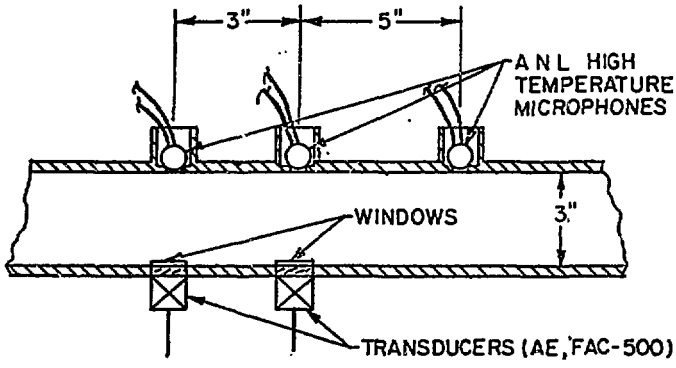

Fig. 3. Acoustic Test Section for Background Noise Measurement

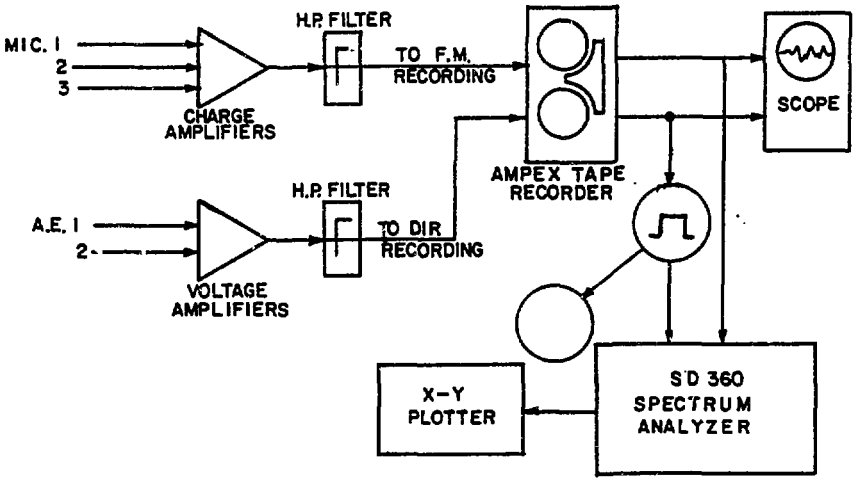

Fig. 4. Data Acquisition and Analysis Systems

Table 1. Solid/Gas Flow Test Conditions

1.	Particle diameter	~1 mm
2.	Temperature	20°C
3.	Mass Flow	0.45, 0.9, 1.35 kg/s
4.	Air Flowrate	7.6×10^{-2} to 1.07×10^{-1} m^3/s
5.	Signal Conditioning	40 dB gain, 1 kHz High Pass

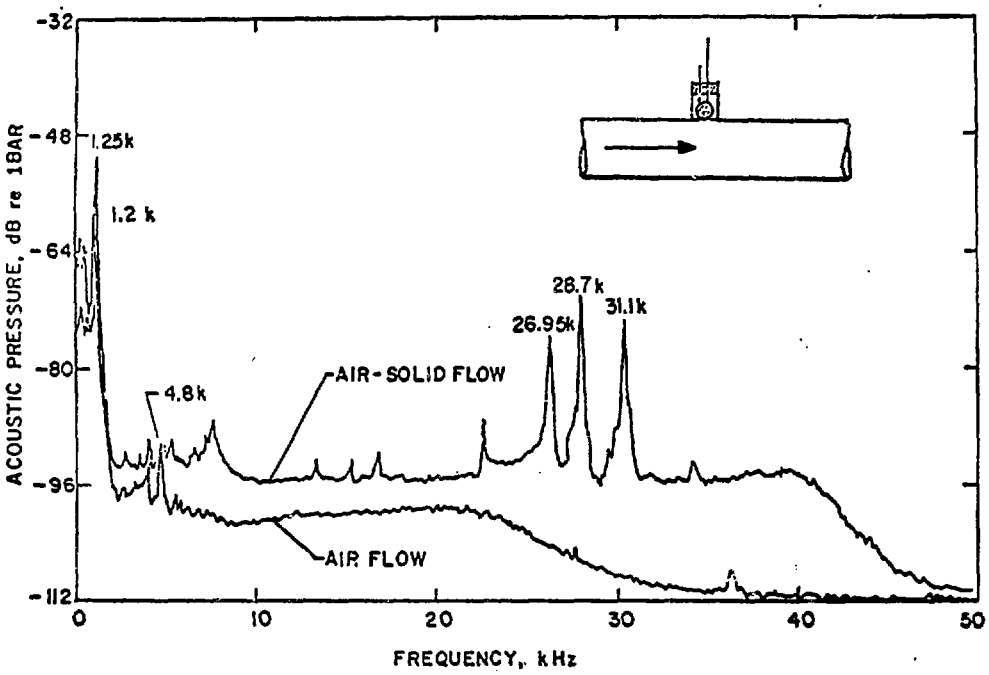

Fig. 5. Acoustic Noise Spectra of Air and Air/Limestone Flows. Signals were detected by the ANL high-temperature microphones with an arrangement similar to that used at BI-GAS. Note that particle noise is at least 10 dB greater than the noise generated by the air flow.

spectrum of the flow noise by at least 10 dB up to about 25 kHz, beyond which the air flow noise decreased drastically. The frequency at which the air flow noise declines is related to the air flowrate and may be used to monitor the air flowrate. Another distinct feature appearing in the spectra is the tone bursts. The tone at 1.2 kHz in the noise spectrum of air flow is shifted to 1.25 kHz for the limestone/air flow. This tone could be related to the resonance frequency of the microphone housing (25.4 cm deep). The shift might be attributed to accumulation of limestones inside the housing. Tones in the 30-kHz region, detected only in the solid/gas flow, are directly related to particle impacts on the microphone.

As shown in Fig. 6, the real-time microphone signals display large pulses arising from direct particle impingement. Two pulses were detected by two microphones separated by 3 in., however, the pulses do not correlate with particle velocity in any way; rather, they are caused by the impact of particles trapped inside the microphone housings. The frequency of impact on a microphone may indicate solids concentration, but this was not investigated. As shown in the figure, the pulses saturated the microphone; thus, for particle velocity measurement, the microphone must be protected from direct particle impingements. We also found that limestone collected inside the microphone housing and eventually altered the sensitivity of the microphone. In view of the difficulties encountered by the microphone sensing, the use of acoustic windows to isolate the sensor from solids was the logical approach.

Two types of window material, stainless steel (SS) 304 and teflon, were tested. The teflon window is softer than the SS window, so higher acoustic attenuation is expected. Consequently, less acoustic energy can be transmitted through the teflon. This is clearly shown in Fig. 7; significant reduction in acoustic energy was detected by the teflon window for frequencies greater than 30 Hz. However, we chose the SS window in this study in order to include high-frequency information as much as possible. In Fig. 8, we plot the power spectra of airflow noise and limestone/air flow noise at two flow velocities under a similar solid feedrate, ~0.45 kg/s. The noise level was much higher for limestone/air flows than for air flows, particularly beyond 10 kHz. Also, the spectra were free from tones due to direct particle impacts. More significantly, we found that the noise level increased with the flowrate and that the increase was distributed over the entire spectrum. This discovery means that bandpass noise can be related to particle velocity.

To illustrate the relation, we measured the noise levels in the range of 10-50 kHz by means of a true root-mean-square (RMS) voltmeter (HP3403C, 0.4% in accuracy). We also computed the autocorrelations of the bandpassed signals on a spectrum analyzer (SD360). The autocorrelation at zero time displacement is equal to the mean square of the signal (or square of the RMS value). For better resolution, we used the autocorrelation values to represent the noise levels. The results are summarized in Table 2. The

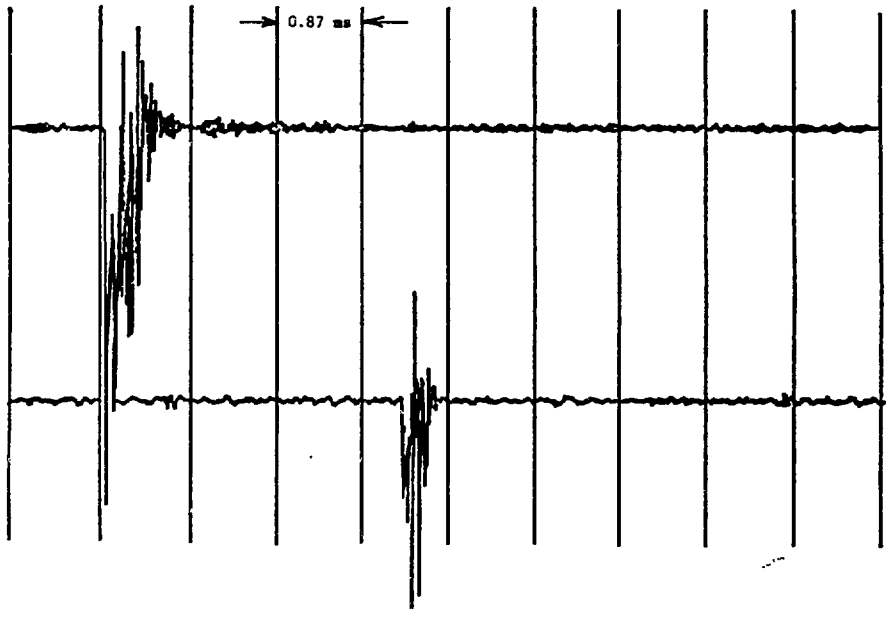

Fig. 6. Real-Time Noise Pulses Detected by Two Microphones Separated by 7.6 cm. The two signals are separated by 3.06 ms, which, however, does not correspond to the particle travel time estimated from the downstream capacitance meter.

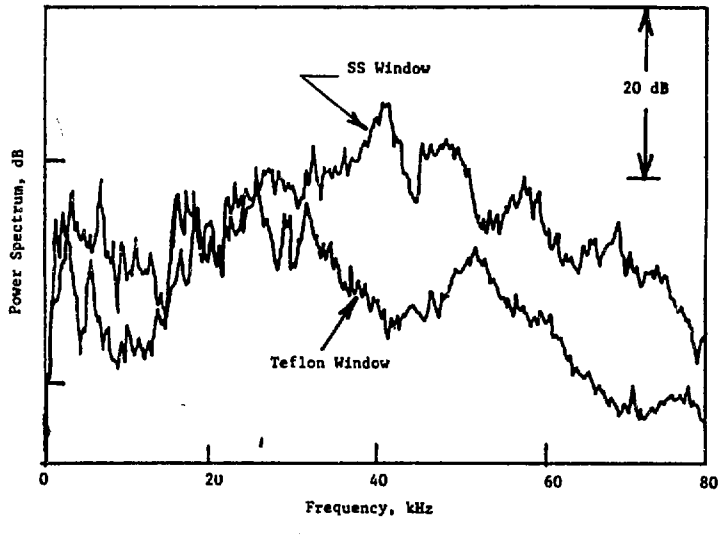

Fig. 7. Power Spectra of Solid/Gas Flow Noise Detected by Two Transducers with Different Acoustic Windows

Table 2. Limestone and Air Flow Test Results: RMS Voltages and Autocorrelation Counts of Acoustic Noise

Mass Flow, kg/s	(lb/s)	Air Flow, m^3/s	(CFM)	Solid Velocity,[a] m/s	(FPS)	RMS Voltage, mV	Auto-correlation Counts
	0	7.6×10^{-2}	(162)	-	-	5.4	1,083
	0	8.3	(176)	-	-	7.8	2,446
	0	9.0	(191)	-	-	12.2	6,088
	0	9.9	(210)	-	-	18.4	13,488
0.55	(1.21)	7.6	(162)	17.6	(57.9)	224	20,825
0.52	(1.15)	8.3	(176)	19.8	(64.9)	278	30,050
0.51	(1.13)	9.0	(191)	21.8	(71.6)	361	53,750
0.52	(1.15)	9.9	(210)	27.3	(89.5)	407	67,350
0.99	(2.18)	7.8	(166)	16.1	(52.7)	202	65,500
0.93	(2.04)	8.9	(190)	20.9	(68.7)	321	165,000
1.02	(2.24)	10.0	(212)	30.8	(101.1)	340	179,000
1.34	(2.96)	7.9	(167)	14.3	(47.1)	210	68,900
1.43	(3.14)	8.7	(184)	15.7	(51.6)	240	92,300
1.48	(3.26)	9.2	(195)	18.5	(60.7)	280	120,300

[a]Solid velocity was provided by J. Bobis using a capacitive flow instrument installed downstream of the acoustic test section during the test series.

32 ensemble average for air flow noise measurement
256 ensemble average for solid-air flow noise measurement

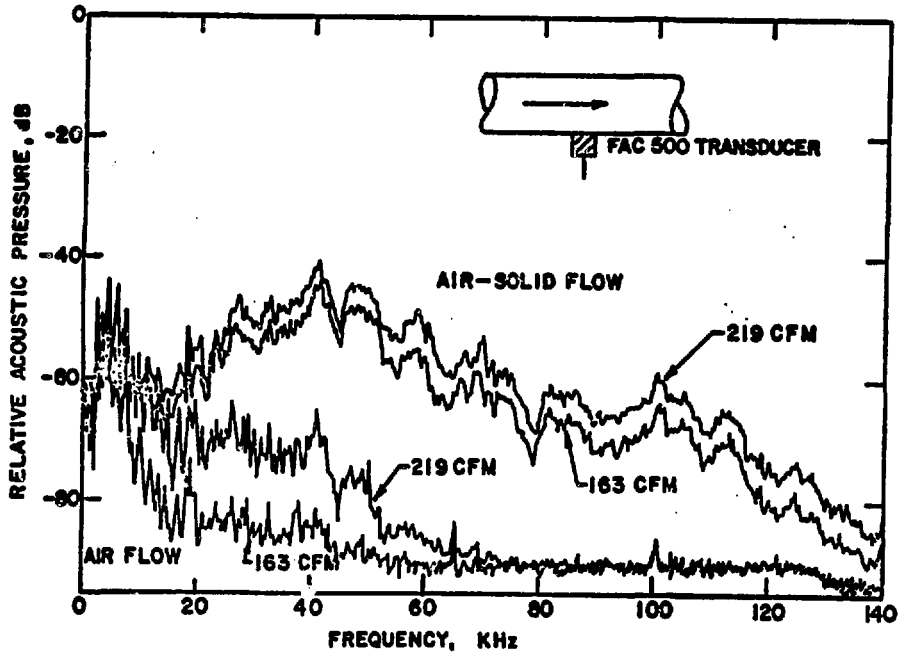

Fig. 8. Acoustic Noise Pressure vs. Frequency for Air Flows and Solid/Air Flows

data are divided into four sets according to the mass flow. In each set, the air flowrate was varied, causing the particle velocity to change accordingly, as indicated by the solid velocity data obtained by the ANL capacitive flow instrument. Data were also plotted in their logarithmic expressions, as given in Fig. 9, in order to establish the power dependence (n) in an empirical relation given as

$$\bar{P} = xu^n \tag{1}$$

where x is a constant, $\bar{P}$ represents the measured acoustic power in terms of autocorrelation, and u is the air flowrate or the particle velocity. In Fig. 9, we plot the logarithm of the autocorrelation at t = 0 versus the logarithm air flowrate, which is assumed to be the terminal particle velocity. From the plots the power factors are estimated; they range from 4.0 to 5.0 for solid suspensions and are ~10 for air flows. This agrees with the model predictions given later. However, in this test series, because of the short test region, the limestone particles could not reach their terminal velocity due to the incomplete acceleration. In Fig. 10, we plot, instead of the air flowrate, the particle velocity measured by the capacitive instrument versus the auto-correlation counts. A smaller power dependence, n, is derived. The result suggests that one may use the value of n to estimate the velocity slip between solids and air. The data shown in Figs. 9 and 10 also indicate that the noise level is proportional to the solid feedrate.

3.1.2 Qualitative Interpretations

In this section, we correlate the results we obtained with existing theroretical models so that we can determine qualitatively the primary sound sources in a solid/gas pipe flow. We address three main subjects: (1) the location of the sound source, at the wall or in the flow, (2) the velocity-dependent air flow noise, and (3) the velocity-dependent solid/air flow noise.

To answer the first question, we must examine how sound is transmitted to a clamp-on piezoelectric transducer through an acoustic window. Figure 11 shows a simplified one-dimensional sensing geometry in which three acoustic media, characterized by their acoustic impedances, are considered. We assume that the interface between the flow and the window has the coordinate x = 0 and that the incident acoustic plane wave is propagating in a direction normal to the interfaces between the media. The wave equations, omitting the trivial time factor $e^{j\omega t}$, in the media can be given as follows:

In medium 1,

$$P_1 = p_1 + p_1' = A_1 e^{-jk_1x} + B_1 e^{jk_1x}, \tag{2}$$

in medium 2,

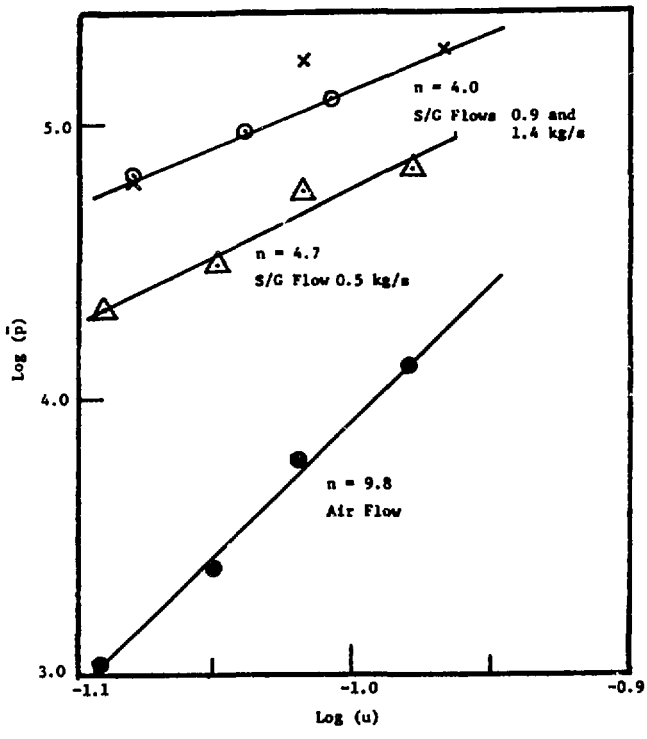

Fig. 9.

Logarithmic Noise Level Taken in Auto-Correlation vs. Air Flowrates for 0, 0.5, 0.9, and 1.4 kg/s Solid Loadings

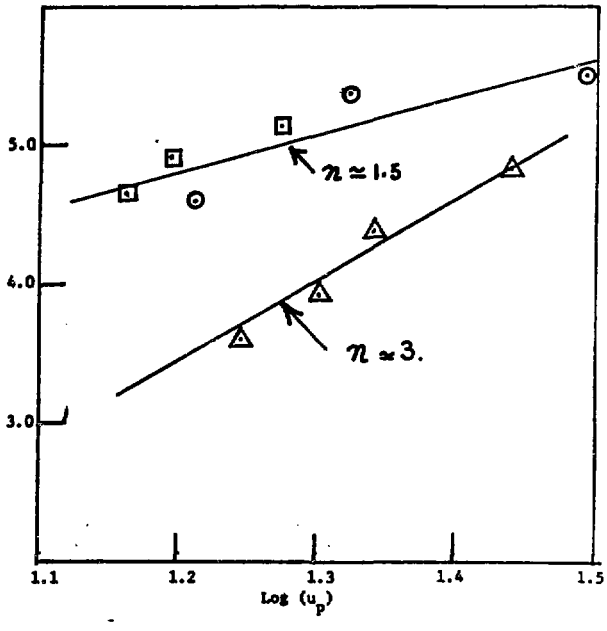

Fig. 10.

Logarithmic Autocorrelations vs. Particle Velocities for Solid/Gas Feedrates of 1, 2, and 3 kg/s

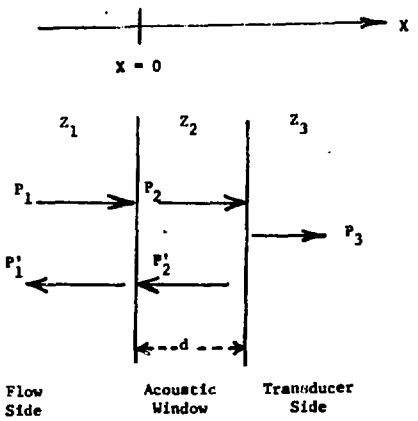

Fig. 11.
One-dimensional Sensing Geometry. Z_i represents the acoustic impedance, P_i the pressure wave traveling in the positive x direction, P_i' the reflected wave, and d the thickness of the acoustic window.

$$P_2 = p_2 + p_2' = A_2 e^{-jk_2x} + B_2 e^{jk_2x} \tag{3}$$

and in medium 3,

$$P_3 = p_3 = A_3 e^{-jk_3x} \tag{4}$$

where k_i is the wave number in the ith medium, and A_i and B_i are amplitudes of the waves. Two additional assumptions have been made in the above equations: (1) that the wave reflected from the transducer is neglected and (2) that A_2 and B_2 represent composite amplitudes after multiple reflections at the window boundary. The boundary conditions applied to this system are:

$$(P_1)_{x=0} = (P_2)_{x=0} \tag{5}$$

$$(V_1)_{x=0} = (V_2)_{x=0} = 0 \tag{6}$$

$$(P_2)_{x=d} = (P_3)_{x=d} \tag{7}$$

$$(V_2)_{x=d} = (V_3)_{x=d} = 0 \tag{8}$$

The boundary conditions are based on the continuity conditions for pressure and velocity (V_i). Substituting the boundary conditions to the wave in Eqs. 2-4, we obtain Eqs. 9-12 relating the amplitudes.

$$A_1 + B_1 = A_2 + B_2 \tag{9}$$

$$A_1 - B_1 = \xi_{12} (A_2 - B_2) \tag{10}$$

$$A_2 e^{-jk_2d} + B_2 e^{jk_2d} = A_3 e^{-jk_3d} \tag{11}$$

and

$$A_2 e^{-jk_2d} - B_2 e^{jk_2d} = \xi_{23} A_3 e^{-jk_3d} \tag{12}$$

where

$$\xi_{ij} = \rho_i C_i / \rho_j C_j \tag{13}$$

As a result of these boundary conditions, we obtain the transmission coefficients from medium 1 to 3, T_{13}, and from 2 to 3, T_{23}, as follows:

$$T_{13} = \frac{A_3}{A_1} = \frac{4\, e^{-jd(k_2 - k_3)}}{5_{1-\Sigma_{12}{}^0} e^{-2jk_2d} + 5_1 + \Sigma_{23}{}^0 \left[\left(1 - e^{2jk_2d}\right) + \xi_{12}\left(1 + e^{2jk_2d}\right)\right.} \tag{14}$$

$$T_{23} = \frac{A_3}{A_2} = \frac{2\, e^{-jd\,(k_2 - k_3)}}{1 + \Sigma_{23}} \tag{15}$$

For the case of using an SS acoustic window, the acoustic impedence in SS is much greater than that in air; thus, $\xi_{12} \doteq 0$ and the transmission coefficients of real amplitude can be given as

$$A_3/A_1 = 4/\gamma^{1/2} \tag{16}$$

where

$$\gamma = [1 + 4\,(1 + \xi_{23})\,\mathrm{Sin}\, k_2d\,\mathrm{Sin}\, 3k_2d + 4\,(1 + \xi_{23})^2\,\mathrm{Sin}^2\, k_2d] \tag{17}$$

and

$$A_3/A_2 = 2/(1 + \xi_{23}) \tag{18}$$

It can be easily shown that $A_3/A_1 \leq 4$ and $A_3/A_2 \leq 2$. Hence, the pressure amplitude transmitted into the third medium, the transducer, is twice the pressure in the acoustic window and four times the pressure of the incident wave in front of the window. However, the acoustic power that the transducer receives is only $A_3^2/\rho_3 C_3$, which is negligible in comparison with the incident acoustic power, $A_1^2/\rho_1 C_1$, because in the power ratio given in Eq. 19, the factor ξ_{13} is approximately zero:

$$\text{Power ratio} = 16\ \xi_{13}/\gamma \tag{19}$$

A piezoelectric transducer is a force-sensitive device; therefore, it can measure the acoustic pressure exerted on the acoustic window. The preceding derivation indicates that both flow-induced noise and direct particle impact force are measurable acoustics. The acoustic impedance mismatch between the gas flow and pipe wall limits the transmission of acoustic energy but an acoustic pressure wave still can be transmitted.

Noise generated by air flow in a duct has been the subject of many investigations [23-26]. It is generally believed that sound pressure is generated from the flow instability in a turbulent fluid. The total sound field radiated by boundary-layer turbulence is a sum of the quadrupole sources in the bulk of the turbulence and the dipole sources at the solid boundary. The acoustic powers due to the dipole and quadrupole sources are proportional to the sixth and eight powers respectively, of the Mach number (M).

Results from this work, as given in Fig. 8, show a higher dependence on the Mach number, $M^{9.8}$, than that of a quadrupole source. This may be explained as follows. First, the sound source is probably a quadrupole source radiating from the air nozzle near the mixing tee. Because the transducers are located near the mixing tee, the nozzle noise would be the primary sound source in that region. The deviation from M^8 dependence may be attributed to the frequency range chosen in this work. Most work in the past concentrated on low-frequency ($\leq$ 10 kHz) acoustics. The 10-50 kHz region has never been examined. It was reported [24], however, that the dependence, n, increases as the frequency band increases to the higher side of the spectrum.

Noise in a solid/gas pipe flow has never been examined in terms of the mechanism of noise generation. Intuitively, the predominant sound sources are the impact noise due to particle/wall and particle/particle collisions. The transient sound radiated by two colliding spheres was experimentally investigated by Nishimura and Takahashi [27]. They showed that the peak pressure amplitudes are proportional to the velocity of impact raised to the 1.2 power. This result agrees with the estimation based on the Hertz law of contact [28] by which the mechanical impact force is derived as

$$f(t) = C_1\ V^{1.2}\ \text{Sin}^{3/2}\ (C_2\ Vt) \tag{20}$$

where V is the particle velocity and C_1 and C_2 are constants. Equation 20 gives the force-time relation for a single particle/particle or particle/

wall collision. To estimate the noise in a solid/gas flow, one must also consider the collision rate. With N as the number of collision per unit of time, the overall impact force becomes

$$F(t) = C_1 \sum_{i=0}^{N} V_i^{1.2} \, \mathrm{Sin}^{3/2} (C_2 V_i t + \phi_i) \tag{21}$$

where ϕ_i represents the ith phase angle. If we assume a uniform particle velocity for qualitative prediction, Eq. 21 may be approximated by

$$F(t) \simeq C_1 N V^{1.2} \, \mathrm{Sin}^{3/2} (C_2 Vt + \phi) \tag{22}$$

The collision rate, N, is a function of particle concentration (i.e., the number of particles per unit of volume), particle diameter, and the relative velocity between the colliding particles [29]. For a qualitative analysis, similar to the treatment in gas kinetics, the collision rate for particle/particle collision may be given as

$$N = C_3 V n_p^2 \tag{23}$$

and for particle/wall collision as

$$N = C_4 V n_p \tag{24}$$

where C_3 and C_4 are constants, and n_p is the particle concentration.
Combining Eqs. 22-24, we obtain

$$F(t) \propto V^{2.2} n_p^{\ell} \, \mathrm{Sin}^{3/2} (C_2 Vt + \phi) \tag{25}$$

where ℓ equals 1 for particle/wall collision and 2 for particle/particle collision. Finally, the transducer response in terms of autocorrelation $\psi(t)$ [30] can be expressed as

$$\psi(0) \sim \frac{1}{4} \frac{\hat{F}(k)}{k^2 \beta} \tag{26}$$

where β is the damping of the system, k the angular frequency, and

$$\hat{F}(k) = \int_{-\infty}^{\infty} \overline{F(t)\,F(t+\tau)}\, e^{-ik\tau}\, d\tau \qquad (27)$$

the power spectral density of the forcing function. Therefore, the auto-correlation at t = 0 is proportional to $V^{4.4}$, which agrees fairly with the present measurement.

Without knowing the characteristics of the transient collision noise, we cannot easily conclude whether the sound is radiating from the particle/particle collisions or the particle/wall collisions. If the latter is assumed, we may be able to explain the variation of magnitude for different mass flows. Intuitively, one would expect that the frequency of particle/wall impacts increases up to a maximum, because of the finite area of the acoustic window, as the particle concentration increases. This may explain why the same sound level was observed for 0.9 and 1.4 kg/s solid feedrates.

3.2 ACOUSTIC CORRELATION MEASUREMENT

The cross-correlation scheme is widely used for measuring the transit time of a moving medium. The technique, coupled with acoustic/ultrasonic sensing, has been developed [31] into a standard method of determining flow velocity in a pipe. It has proven to be an accurate method for velocity measurement in a coal-slurry mixed-phase flow. The acoustic cross-correlation technique requires acoustic waves to be sent into the flow and retrieved in order to process the flow modulation. For solid/liquid flows, the flow modulation originates from density fluctuation. The same acoustic scheme has never been examined for solid/gas flows because of the inherent difficulty of acoustics in a solid/gas system, such as the high sound attenuation in the ultrasonic frequency range and the strong solid impact noise.

During the early stage of this developmental program, we focused on developing an intensive sound source to generate a sound wave at a frequency of around 100 kHz or higher. High-frequency acoustic waves were desired for their sensitivity in detecting solids in the stream. Two sound sources were investigated: (1) a stem-jet sound source (see App. A) and (2) the acoustics generated by a piezoelectric crystal [32]. Both sources were unsuccessful for use in monitoring solid/gas flows because of the poor signal-to-noise ratio. Moreover, the stem-jet source introduced additional air flow into the main flow stream, which was undesirable.

A novel acoustic sensing concept was later introduced. Instead of transmitting sound waves through the flow medium, the new method detects chiefly the noise that interacts with the acoustic field established within the pipe wall. Since the noise may be related to the particle concentration, as discussed earlier, the noise-modulated sound field in the pipe wall may contain the specific flow information arising from particle

concentration variation. Therefore, cross-correlating the noise modulation may deduce a velocity-dependent correlation function.

3.2.1 Description of Instrument and Flow Tests

Figure 12 shows the acoustic cross-correlation test section developed at ANL. Two pairs of transducers (AE FAC-500) were clamped directly onto the pipe. In each pair, one transducer acted as a transmitter and the other as a receiver. The separation between the pairs was 6.5 cm, slightly larger than the pipe diameter. To avoid acoustic cross talk and noise pickup from the loop, Viton gaskets were inserted between flanges. Cross talk and noise pickup were reduced by at least 60 dB as a result. The test section was installed 8 m downstream of the mixing tee at the dilute-phase horizontal test region during the flow tests with glass beads.

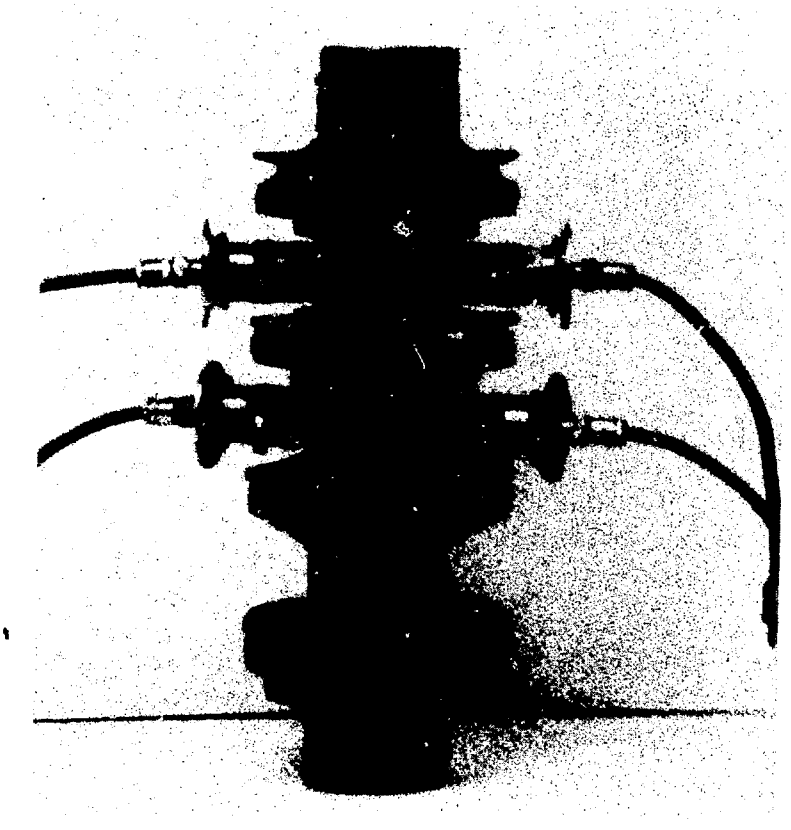

Fig. 12. Acoustic Cross-Correlation Test Section for Solid/Gas Flow Tests

Figure 13 outlines the electronics used to supply and condition the signals. The transmitters were typically excited by a continuous wave of a frequency between 800 kHz to 1 MHz and with the power of 1 watt. Received signals were conditioned by bandpass amplifiers set at a gain of 40 dB and a bandwidth of 100 kHz to 1 MHz. A synchronous detector (AD360) was used to demodulate the conditioned signals before they were recorded onto a magnetic tape. When the data were analyzed, signals, identified by the index number recorded on the voice channel, were fed into bandpass filters to select the best frequency range leading to a cross-correlation function of good precision. The cross-correlation was computed on a real-time, 1024-point, spectrum analyzer. Table 3 outlines the test matrix of the glass beads and air flow test. The test covered a range of mass flow from 1 to 4 pps, corresponding to solid-to-gas loading ratios of 6 to 22. The air velocity was measured at the inlet orifice; because of relatively low loading, we expected very little variation in air velocity through the entire test region. In other words, the energy used to accelerate particles was negligible. The significant feature of this test was the incorporation of a radioactive particle experiment. Two gamma detectors were positioned immediately upstream and downstream of the acoustic instrument, so that a direct comparison of the two measurements was possible. The particle velocities in Table 3 were measured by the radioactive particle TOF technique. Each velocity represents an average of 15 radioactive particles passing through the acoustic instrument.

3.2.2 Results and Discussion

Data were analyzed with an analysis range of 5 kHz, corresponding to 0.1 ms in the time resolution. Each correlation function resulted from 256 ensemble averages, which equal about 15 s in real time. The maximum of a correlation function was located by manually moving the cursor. The maximum was used as the average particle transit time between the two sensing transducers whose separation was assumed to be the average travel length for the particles. Finally, the velocity was derived from the transit time at the peak maximum. The range of the transit time measured in this test was between 3 and 5 ms; thus, the time resolution was better than 4%. The peak width of a cross-correlation is determined by the velocity spread, filtering setting, and sensor width. The sensor width can be estimated from the test-section construction, which gives the separation of the two sensing regions from 3.5 cm to 9.5 cm. Hence a width of ~3 ms may arise from the separation. The actual measured width is greater than 3 ms because of the filtering and the velocity spread. The filtering effect can be minimized by taking a bandwidth much larger than the signal bandwith.

In Table 4, we summarize the results of particle velocity measurement. Three frequency bands were chosen in the analysis. In general, increasing the low-pass cutoff frequency from 30 to 500 Hz improved significantly the measurement statistics; the standard deviation was better than 5% for measurements using a 500-Hz low-pass setting. Another trend

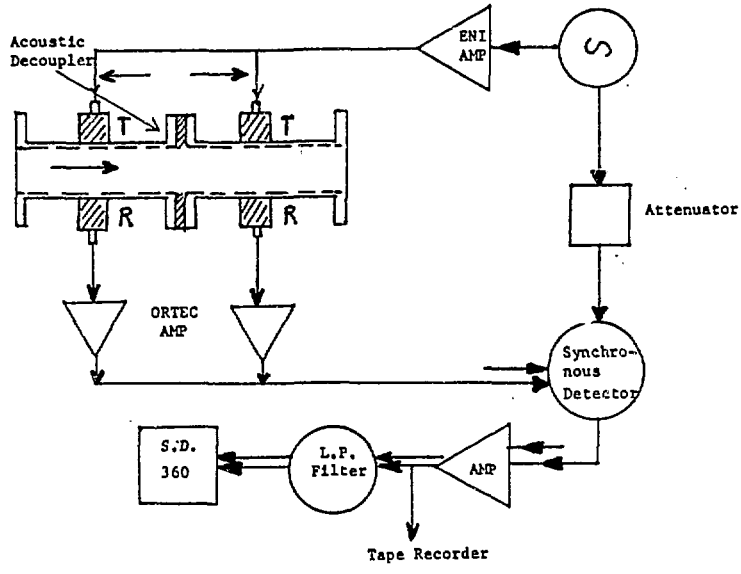

Fig. 13. Active Acoustic Cross-Correlation Sensing Arrangement and Associated Electronics

Table 3. Glass Beads[a] and Air Flow Test Conditions

Run	Data Index	Mass Flow, kg/s	(lb/s)	Velocity Air,[b] m/s	Solid-to-gas Loading	Particle Velocity at Acoustic Test Section m/s
109	39-71	1.45	(3.2)	30.3	16.6	24.0
110	26-74	0.86	(1.9)	30.0	10.2	23.0
111	45-68	2.0	(4.4)	29.6	22.0	23.7
112	24-75	0.5	(1.1)	28.3	6.5	19.9
113	40-66	1.73	(3.8)	38.1	16.6	29.0
114	32-67	1.22	(2.7)	38.1	10.8	28.7

[a] Glass beads are 1 mm in diameter and 2.46-2.49 g/cm^3 in density.

[b] In a 2 in. Schedule 40 pipe.

observed was the shift of the cross-correlation peak toward low transit time or high particle velocity as the low-pass frequency was reduced. Figure 14 illustrates the peak shift and the shape variation of the correlation functions. The reason for the drastic reduction in transit time at 30 Hz may either be that (1) the wavelength of the 30-Hz flow-related signal is much longer than the transducer spacing, thus causing the signals to be correlated within the same wave quadrant [33] or (2) that a low-frequency flow phenomenon dominates the correlation function, thus obscuring the true correlation peak. It was observed that for solid feedrates greater than or near 0.9 kg/s signals exhibit an oscillatory (~20 Hz) structure. Figure 15 shows an example of the flow oscillation at 0.86 kg/s in the solid feedrate. The oscillation may result from the non-pulsating transport phenomenon due to the mixing-tee arrangement. To resolve a true correlation function, one must use a high-pass filter to reduce the tone structure. Figure 16 shows a series of cross-correlation functions obtained with a 30-500 Hz bandwidth. The correlation peaks are more or less symmetrical around the maximum, implying a uniform velocity distribution for particles being detected.

Table 4. Particle Velocity, V_A, Measured by Acoustic Sensing Compared With the Hot-Sample Measurement V_H

Run	SGL[a]	BW,[b] Hz	V_A,[c] m/s (σ)[d]	V_H,[e] m/s	V_A/V_H
112	6.5	1-30	NR[f]	19.9	-
		1-100	12.4 (0.82)	19.9	0.62
		30-500	13.8 (0.54)	19.9	0.69
110	10.2	1-30	18.8 (3.7)	23.0	0.82
		1-100	17.8 (3.2)	23.0	0.77
		30-500	15.0 (0.62)	23.0	0.65
114	10.8	1-30	NR	28.7	-
		1-100	33.6 (6.0)	28.7	1.17
		30-500	18.5 (0.52)	28.7	0.64
113	14.6	1-30	NR	29.0	-
		1-100	33.3 (17.3)	29.0	1.15
		30-500	19.4 (0.84)	29.0	0.67
109	16.6	1-30	24.3 (8.6)	24.0	1.01
		1-100	20.7 (4.5)	24.0	0.86
		30-500	15.3 (0.44)	24.0	0.64
111	22.0	1-30	NR	23.7	-
		1-100	38.5 (9.0)	23.7	1.62
		30-500	15.2 (0.38)	23.7	0.64

[a] Solid-to-gas loading ratio.

[b] Bandwidth of the signal.

[c] Particle velocity measured by acoustic sensing.

[d] Standard deviation.

[e] Particle velocity by radioactive TOF.

[f] Not resolved, poor SNR.

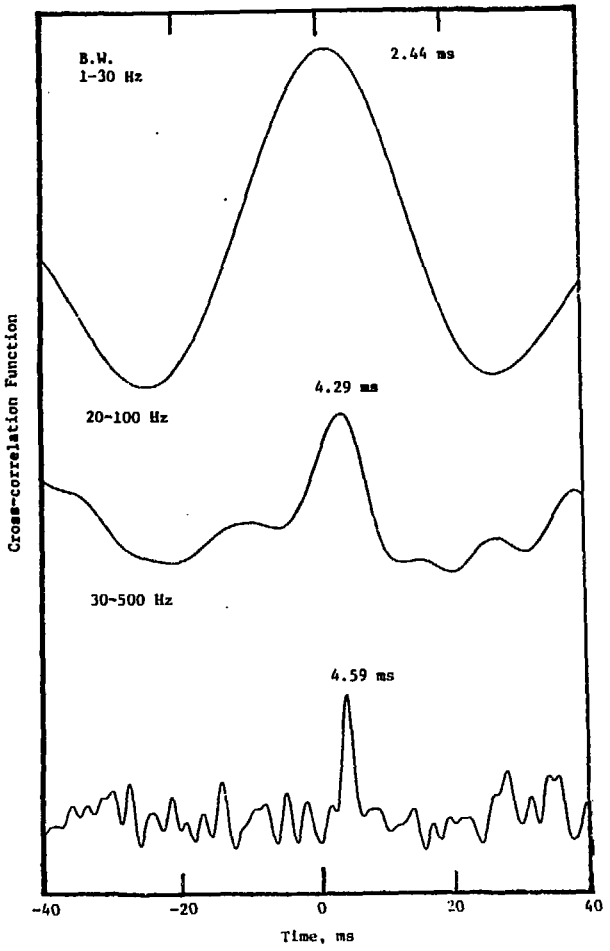

Fig. 14. Cross-Correlation Functions Obtained with Different Filter Bandwidths. Data correspond to a solid-to-gas loading of 10.2.

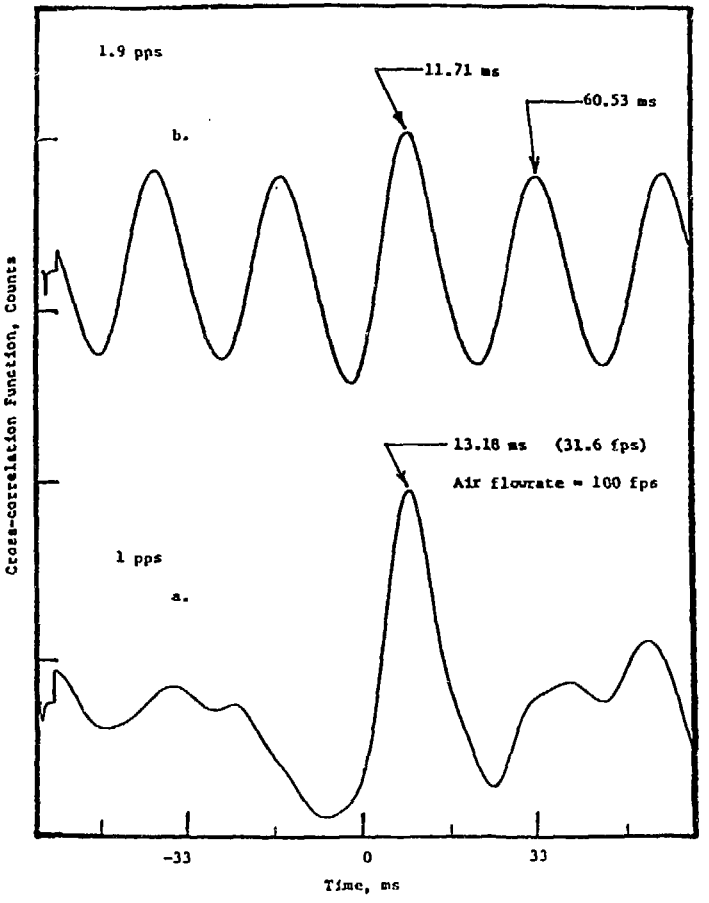

Fig. 15. Cross-Correlation Functions Detected by the Active Acoustic Cross-Correlation Technique Applied to Solid/Gas Flows at Solid Loadings of (a) 0.45 kg/s and (b) 0.86 kg/s

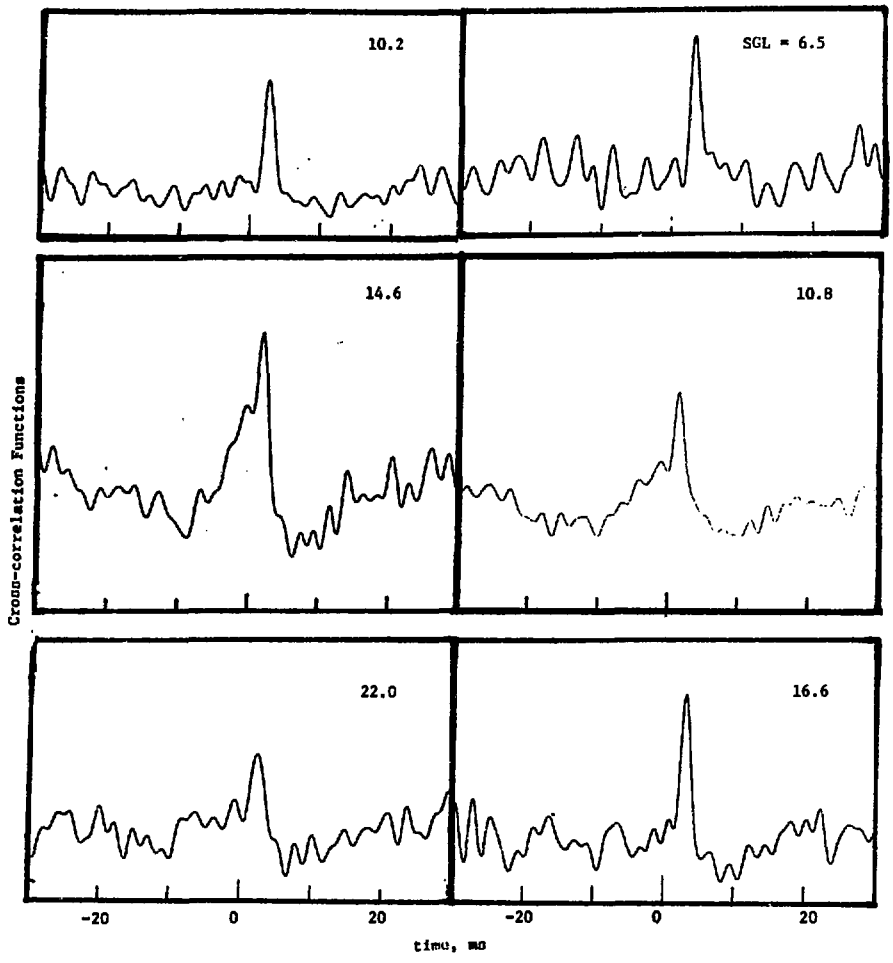

Fig. 16. Cross-Correlation Functions of Signals from Different Solid-to-Gas Loadings

In general, we found that the cross-correlation functions were resolved better for low solid-to-gas loadings. As the loading increased, the correlation peak was broadened, especially at the base of the peak. This may be caused by the instability of the solid flow; possibly, solid settling may be occurring. At the highest solid loading (22), the correlation peak strength was considerably reduced, again indicating that the particle flow was not steady at this loading.

Particle velocity data derived from the correlation peaks differed significantly from the velocities measured by the radioactive TOF technique. However, the difference remained the same over the whole test matrix if a 30-500 Hz bandwidth was used. The relation between the two measurements techniques is given as

$$V_H = 1.53 \quad V_A \tag{28}$$

where V_H and V_A represent the measured particle velocities by radioactive and acoustic techniques, respectively. Figure 17 displays the relation of Eq. 28 using the data given in Table 4. The accuracy of the acoustic method, after applying the constant factor (1.53), is near 3%.

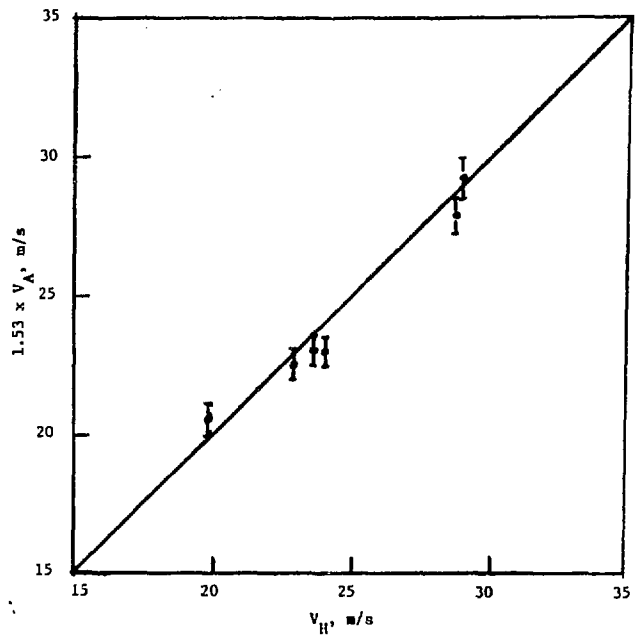

Fig. 17. Comparision of Particle Velocities (V_A) Sensed by the Acoustic Method vs. the Radioactive Particle Injection Method

The 1.53 factor may be attributed to the difference in the flow region sensed by the two methods. Laboratory experiments [34,35] have shown that in the absence of electrostatic forces, solid particles concentrate toward the center of the pipe. However, the acoustic instrument mainly detects solids near the pipe wall. Based on the model calculation of Michaelides [36], the difference between the velocities in the turbulent region and the viscous sublayer is about 3:1 for a solid-to-gas loading ratio of 6. Extrapolating that result to the present loading ratios, a difference or 1.5:1 in the velocities is definitely possible. Therefore, we believe that the active cross-correlation instrument really measures the particle velocity in a region near the pipe wall. The velocity thus requires a multiplier of ~1.53 to bring it into agreement with the average particle velocity.

4. CONCLUSIONS AND FUTURE DEVELOPMENT

In this report, we explain two acoustic/ultrasonic sensing techniques that can be applied to particle-velocity measurement in a solid/gas pneumatic transport line. One technique, passive in nature, simply measures the bandpassed acoustic noise level, produced by particle/particle and particle/wall collisions. The noise levels, given in true RMS voltages or in autocorrelations, show a linear relationship to particle velocity and increase with solid concentration up to 0.9 kg/s for the present mixing arrangement. Therefore, the passive technique requires calibration and a separate measure of solid concentration before it can be used to monitor particle velocity. The second technique is based on the active cross-correlation principle. It provides a direct particle velocity measurement by correlating flow-related signatures at two sensing stations. The velocity data obtained are consistently smaller than those measured by the radioactive-particle TOF method. A multiplier of 1.53 is required to bring the acoustic data into agreement with the radioactive result. The difference originates from the different flow fields in which particles are detected. Since the radioactive method senses particles mainly in the turbulent region, it essentially measures the average particle velocity across the pipe. The acoustic technique detects particles near the pipe wall, and hence measures particle velocity in the viscous sublayer.

Based on the present test, which covers solid-to-gas loading ratios ranging from 6 to 22 and flow velocities of 20 to 30 m/s in a 2 in. pipe, the multiplier remains a constant. Thus, the acoustic cross-correlation technique could potentially be used in industrial applications because of its nonintrusive nature, safety, economic attractiveness, and convenience. However, further research and development are needed in the following areas: (1) effects due to particle size and pipe diameter, (2) detection limits and accuracy in particle velocity and solid loading, and (3) design of the instrument and an integrated electronic system. Finally, combination of the passive and active techniques needs further development for mass-flow control in a pneumatic transport line.

ACKNOWLEDGMENTS

We wish to acknowledge the contributions of W. E. Brewer, W. P. Lawrence, and L. T. Bernovich for operating the ANL SGFTF during the solid/gas tests. We thank Drs. J. P. Bobis and K. G. Porges for providing the capacitance meter and radioactive TOF measurement results. We also acknowledge the management support for Mr. R. S. Zeno and Dr. M. Petrick of ANL. We thank N. Heeg for typing the report, and P. Chen for technical editing.

REFERENCES

1. A. Fortier and C. P. Chen, "Ecoulement turbulent stationnaire biphasique air-solide dans un tube cylindrique, a forte concentration massique," J. de Mecanique 15 (1) (1976).

2. S. L. Lee and J. Srinivasan, "Measurement of Local Size and Velocity Probability Density Distributions in Two-phase Suspension Flows by Laser-Doppler Technique," Int. J. Multiphase Flow 4, 141 (1978).

3. G. A. Irons and J. S. Chang, "Particle Fraction and Velocity Measurement in Gas-powder Streams By Capacitance Transducers," Int. J. Multphase Flow 9 (3): 289 (1983).

4. J. P. Bobis et al., "Performance Characteristics of a Capacitive Flowmeter on the ANL Solid/Gas Flow Test Facility," Argonne National Laboratory Report ANL-82-62, CONF-820612 (1982).

5. S. L. Soo, "State of Multiphase Instrumentation," Developments in Theoretical and Applied Mechanics, XI, 563 (1982).

6. T. J. Brain and P. W. W. Scott, "Survey of Pipeline Flowmeters," J. Phys. E : Sci. Instrum. 15 (1982).

7. S. Nieh, B. T. Chao, and S. L. Soo, "An Electrostatic Induction Probe for Measuring Particle Velocity in Suspension Flow," International J. of Particulates and Science (1985).

8. H. B. Karplus, A. C. Raptis, and D. R. Canfield, "Development and Testing of High-Temperature Acoustic Doppler Flowmeters," Argonne National Laboratory Report ANL/FE-81-64 (1981).

9. A. C. Raptis and S. H. Sheen, "Ultrasonic Properties of Coal Slurries and Flow Measurements by Cross Correlation," IEEE Trans. on Sonics and Ultrasonics, SU-28 (4): 248 (1981).

10. A. C. Raptis, "Instrumentation and Control for Fossil Energy," Quarterly Technical Progress Report, Argonne National Laboratory ANL/FE-84-02 (1983).

11. L. R. Dates and J. P. Bobis, "The ANL Solids/Gas Flow Test Facility," Argonne National Laboratory Report ANL/FE-82-22 (1982).

12. A. C. Raptis et al., "Instrumentation and Control for Fossil Energy," Argonne National Laboratory Quarterly Technical Progress Report (Oct.-Dec. 1984).

13. J. P. Bobis, K. G. A. Porges, A. C. Raptis, W. E. Brewer, and L. T. Bernovich, "Particle Velocity and Solid Volume Fraction Measurements with a New Capacitive Flowmeter at the Solid-gas Flow Test Facility," Argonne National Laboratory Report ANL/FE-86-04 (1986).

14. J. P. Bobis, S. H. Sheen, K. G. Porges, H. B. Karplus, M. M. Farahat, W. E. Brewer, N. M. O'Fallon, and A. C. Raptis, "Preliminary Report on Development of Nonintrusive Flow Instrumentation at the ANL Solid-liquid Test Facility," Argonne National Laboratory Report ANL/FE-83-18 (1983).

15. A. C. Raptis, J. W. Fitzgerald, G. F. Popper, R. Doolittle, and S. H. Sheen, "A Feasibility Study of Acoustic/Ultrasonic Flowmeters for Solid/Gas Systems," Argonne National Laboratory Report ANL/FE-49622-TM01 (1978).

16. D. H. Tack, M. W. Smith, R. F. Lambert, "Wall Pressure Correlations in Turbulent Airflow," JASA 48 (4): 410-418 (1961).

17. A. M. Teplitsky; "Electrical Power Plant Noise Emission Controls," Sound and Vibration, p. 24 (Sept. 1976).

18. M. Arrington, "The Use of Acoustic Emission Instrumentation to Monitor Powder Flows," NDT International p. 3 (1981).

19. P. D. Roach and A. C. Raptis, "An Acoustic Char Flow Monitor for the BI-GAS Pilot Plant," Argonne National Laboratory Report ANL/FE-49622-TM08 (July 1979).

20. S. H. Sheen and A. C. Raptis, "Density Measurement Studies at the BI-GAS Pilot Plant," Argonne National Laboratory Report ANL/FE-81-57 (1981).

21. A. P. Gavin, T. T. Anderson, and J. J. Janicek, "Sodium Immersible High Temperature Microphone Design Description," Argonne National Laboratory ANL-CT-75-30 (1975).

22. J. P. Bobis et al., "Experimental Results of Capacitive Flowmeter and Analytical Modeling of Solid-gas Flow Mixture at ANL S/GFTF," Proc. Midwest Universities Energy Consortium Conf. on Elect. Utility Research (1984).

23. E. A. Vecchio and C. A. Wiley, "Noise Radiated from a Turbulent Boundary Layer," JASA 53 (2): 596 (1973).

24. E. M. Greshilov and M. A. Mironov, "Experimental Evaluation of Sound Generated by Turbulent Flow in a Hydrodynamic Duct," Sov. Phys. Acoust. 29(4): 275 (1983).

25. G. P. Haddle and E. J. Skudrzyk, "The Physics of Flow Noise," JASA 46(1): 130 (1969).

26. Willi Möhring, Ernst-August Müller, and F. Obermeier, "Problems in Flow Acoustics," Rev. Modern Phys. 55(3): 707 (1983).

27. G. Nishimura and K. Takahashi, "Impact Sound by Mutual Collision of Two Steel Balls," 1965 Bulletin of the Japan Soc. of Precision Eng. 1, pp. 47.

28. L. L. Koss and R. J. Alfredson, "Transient Sound Radiated by Spheres Undergoing an Elastic Collision," J. of Sound and Vibration 27(1): 59 (1973).

29. J. J. E. Williams and R. I. Crane, "Particle Collision Rate in Turbulent Flow," Int. J. Multiphase Flow, 9(4): 421 (1983).

30. A. P. Dowling and J. E. Ffowcs Williams, "Sound and Sources of Sound," John Wiley and Sons, Inc., 1983, p. 239.

31. S. H. Sheen, A. C. Raptis, J. Bobis, Nam Lee, and T. Simpson, "Evaluation of Active Ultrasonic Cross-correlation Technique in Coal/Liquid Pipe Flow Measurements," Argonne National Laboratory Report ANL/FE-85-12 (1985).

32. A. C. Raptis et al., "Instrumentation and Control for Fossil Energy, Quarterly Technical Progress Report, Argonne National Laboratory ANL/FE-84-14 (Jan.-Mar. 1984).

33. S. H. Sheen and A. C. Raptis, "Effects of Low-pass Filtering on the Accuracy of Cross-correlation Velocity Measurement," IEEE, Ultrasonics to be published.

34. S. L. Soo, G. J. Trezeh, R. C. Dimick, and G. F. Honstreiter, "Concentration and Mass Flow Distribution of a Gas-Solid Suspension, Ind. Engng. Chem. Fund. 3, 98-105 (1964).

35. S. L. Soo and J. A. Regalbuto, Concentration Distribution in Two-Phase Pipe Flow, Can. J. Chem. Engng., 38, 160-165 (1960).

36. E. E. Michaelides, "A Model for the Flow of Solid Particles in Gases," Int. J. Multiphase Flow, 10, (1): 61 (1984).

37. "High-Intensity Ultrasound," L. D. Rosenberg, ed., Vol. 1 (1969).

APPENDIX:

STEM-JET WHISTLES

A high-intensity sound source can be built from turbulent jet noise with a proper resonator. The stem-jet whistle[37] is an example. Figure A.1 shows its design. The parameters that control the sound level and frequency are the nozzle-cavity separation, ℓ, the cavity depth, h, and the effective cavity diameter, dr. In principle, the output magnitude is affected by the distance ℓ and the injecting gas pressure. The output frequency can be estimated by

$$f(Hz) = C/[4(h + 0.3\ dr)]$$

where C is the sound speed in the gas.

Two whistles were built and a simple setup was used to determine the frequency spectra of both. A transducer (AE-FAC500) was placed about 1 cm away from each whistle. Pressured nitrogen was used to generate the acoustics. It was found that, for both whistles, the minimum pressure required was about 15 psig. The outputs were analyzed on a spectrum analysis (SD360). Figure A.2 shows the spectra of the whistle outputs. Other than the fundamental frequency, each whistle also produced several harmonics of significant magnitude.

The whistles were also tested with an actual solid/gas flow. However, the test was aborted because of the density disturbance caused by the additional nitrogen injection into the flow from the whistles. Therefore, a modification to bypass the nitrogen injection is needed for useful application to the monitoring of solid/gas flow.

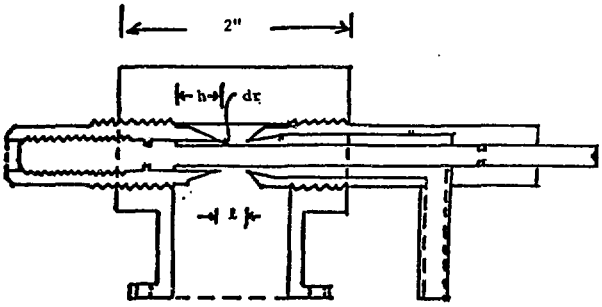

Fig. A.1. Stem-Jet Whistle Design; ℓ is the nozzle-cavity separation, h the cavity depth, and dr the effective cavity diameter.

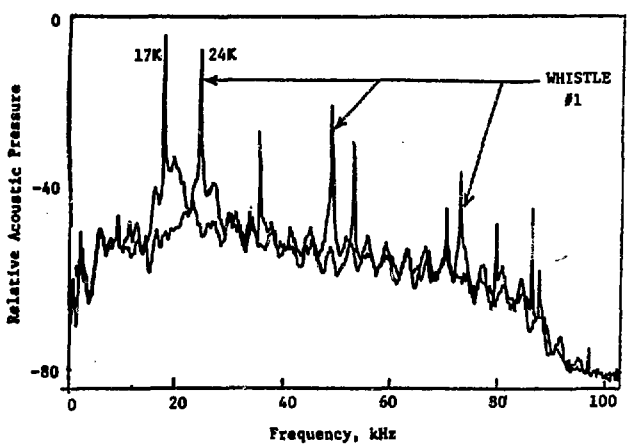

Fig. A.2. Spectra of the Sound Outputs from Two Stem-Jet Whistles

Distribution for ANL/FE-85-07

Internal:

W. E. Brewer
J. P. Bobis
E. D. Doss
H. Drucker
W. A. Ellingson
P. S. Farber
N. Gopalsami
R. E. Holtz
A. B. Krisciunas
W. P. Lawrence
K. M. Myles
N. M. O'Fallon
M. Petrick
W. F. Podolski
A. C. Raptis (10)
S. H. Sheen (6)
M. Srinivasan
C. E. Till
R. W. Weeks
R. S. Zeno
S. K. Zussman
ANL Contract File
ANL Libraries
ANL Patent Dept.
TIS Files (6)

External:

DOE-TIC, for distribution per UC-90a (191)
Manager, Chicago Operations Office, DOE
F. Herbaty, DOE-CH
M. Zahid, DOE-CH
Components Technology Division Review Committee:
P. Alexander, Flopetrol Johston Schlumberg, Houston, Texas
D. J. Anthony, General Electric Company, San Jose, Calif.
A. A. Bishop, U. Pittsburgh
B. A. Boley, Northwestern U.
R. N. Christensen, Ohio State U.
R. Cohen, Purdue U., West Lafayette
R. E. Scholl, URS, San Francisco, Calif.
J. Weisman, U. Cincinnati
D. L. Basdekas, Office of Nuclear Regulatory Research, USNRC
J. Byam, Morgantown Energy Technology Center, USDOE
J. Carr, Office of Fossil Energy, USDOE
C. S. Chen, U. Akron
J. S. Coleman, Office of Energy Research, USDOE
A. C. Dolbec, Electric Power Research Institute, Palo Alto
P. J. Ebert, Office of Energy Research, USDOE
F. Karlson, Electric Power Research Institute, Palo Alto
T. Keech, Morgantown Energy Technology Center, USDOE
J. Kovach, Morgantown Energy Technology Center, USDOE
S. Lee, Pittsburgh Energy Technology Center, USDOE
M. McMillian, Morgantown Energy Technology Center, USDOE
C. Nakaishi, Morgantown Energy Technology Center, USDOE
J. Notestein, Morgantown Energy Technology Center, USDOE
W. H. Piispanen, Battelle-Columbus Laboratories
S. Sami, Southern Illinois U., Carbondale
T. Schmidt, Shell Development, Houston
M. A. Scott, U. Tennessee Space Institute, Tullahoma
F. E. Senftle, U.S. Geological Survey, Washington, D.C.
V. Sethi, Kentucky Center for Energy Research, Lexington
T. Simpson, Office of Fossil Energy, USDOE
M. Singer, Office of Fossil Energy, USDOE
A. B. Tanner, U. S. Geological Survey, Washington, D.C.
O. Tassicker, Electric Power Research Institute, Palo Alto
T. Torkos, Pittsburgh Energy Technology Center, USDOE
E. S. Van Valkenburg, Leeds & Northrup Co., North Wales, PA
J. Wilson, Morgantown Energy Technology Center, USDOE